SURFACE AND INTERFACE ANALYSIS
Surf. Interface Anal. **30**, 161–166 (2000)

XPS characterization of oxide films formed in cobalt-based alloys during corrosion tests at high temperature

C. Maffiotte,* M. Navas, M. L. Castaño and A. M. Lancha
CIEMAT-DFN, Avda. Complutense 22, 28040 Madrid, Spain

Hard-facing cobalt-based alloys, type Stellite-6, are widely used for wear resistance in components of nuclear reactor coolant circuits. In this work, high-temperature (290 °C) corrosion tests have been performed under simulated pressurized-water reactor (PWR) primary heat transport circuit conditions at two different pHs. The corrosion resistance of this alloy was evaluated by weight-loss measurements in long-term tests. Surface analysis of the samples, using x-ray-photoelectron spectroscopy (XPS) and subsequent composition–depth profiles, was performed in order to characterize the oxide films (composition, thickness, etc.) formed during exposure at high temperature. Quantitatively different oxide film thicknesses were detected in the two conditions studied, but only slight qualitative differences were observed in the composition of the oxide layers. In both conditions the results seem to show that the corrosion mechanism of this alloy is characterized by preferential dissolution of cobalt and the formation of a protective chromium oxide film.

KEYWORDS: Stellite; corrosion; XPS; oxide layers; depth profile

INTRODUCTION

Stellite-6 is a cobalt-based alloy that is used frequently as a hard-facing material in the primary heat transport circuit of nuclear reactors. The main property of this alloy is its high resistance to wear, corrosion and erosion. However, because this alloy can suffer corrosion degradation when exposed to operating conditions, it represents a significant source of ^{59}Co to the primary coolant system that can be transformed into radioactive ^{60}Co, thus increasing the radiation fields. Although Stellite-6 only represents 0.03% of the total area of a primary coolant circuit (as wearing material for valves, pumps and other components), it can represent up to 70% of the total cobalt released to coolant.[1]

Previous XPS studies of corrosion behaviour on these materials[2–4] have shown the formation of a chromium-enriched and cobalt-depleted oxide layer, from which it may be deduced that preferential dissolution of cobalt was the main degradation mechanism. The influence of redox conditions on this mechanism has been reported[2–4] in the literature but a lack of information exists about the effect of pH. Considering the possible pH variation during operation of a pressurized-water reactor (PWR) and in order to evaluate its influence on the behaviour of Stellite-6, two primary coolant conditions have been simulated. Weight-loss measurements and x-ray photoelectron spectroscopy (XPS) have been used to characterize the degradation extension and the oxide films.

* Correspondence to: C. Maffiotte, CIEMAT-DFN, Avda. Complutense 22, 28040 Madrid, Spain.
E-mail: cesar.maffiotte@ciemat.es

EXPERIMENTAL

A rod of cast Stellite-6 alloy, 30 mm diameter, was machined by electro-erosion into 3 mm thick discs. After the machining, the specimens were prepared by abrasion with No. 600 silicon carbide paper prior to the corrosion tests. The nominal composition of the alloy (in wt.%) was: 56.66% cobalt, 30.12% chromium, 4.51% tungsten, 2.49% nickel, 2.28% iron, 1.21% molybdenum, 1.13% carbon, 0.83% silicon and 0.77% manganese. The alloy microstructure consists of a cobalt- and chromium-rich solid solution matrix, together with a precipitate phase rich in chromium and tungsten.

High-temperature (290 °C) corrosion tests have been performed under simulated PWR primary heat transport circuit conditions at two different pHs. Experimental work was carried out in a high-temperature and high-pressure recirculating loop. The specimens were exposed to the following environments: solution A (300 ppm H_3BO_3 + 2.65 ppm LiOH + 2 ppm H_2, $pH_{290\,°C}$ 7.4) and solution B (2000 ppm H_3BO_3 + 2 ppm H_2, $pH_{290\,°C}$ 5.05), for periods of 250, 1000 and 2000 h. Corrosion behaviour of the alloy was evaluated by weight-loss measurements and analyses of the oxide layers by XPS.

The XPS analyses were carried out with a Perkin-Elmer PHI 5400 spectrometer equipped with an Mg Kα excitation source ($h\nu$ = 1253.6 eV) and a beam size of 1 mm diameter. The spectrometer was calibrated using copper, gold and silver standards. Typical operation conditions were: x-ray gun, 15 kV, 20 mA; pressure in the sample chamber $\sim 10^{-9}$ Torr; pass energy, 89.5 eV for general spectra (0–1100 eV) and 35.75 eV for high-resolution spectra. In order to take into account the charging effects on the measured binding energies, accurate

Received 15 July 1999
Revised 6 November 1999; Accepted 6 November 1999

binding energies were determined by referencing to the adventitious C 1s peak at 285.0 eV.

Composition–depth profiling was performed by sequential XPS surface analysis and ion sputter etching using a 1.5 keV argon ion flux. The focused ion beam (~2 mm spot size) was rastered over an area of 0.35 cm^2, whereas the average current density (measured with a Faraday cup) was 10 $\mu A\ cm^{-2}$. Calibration of the ion sputter etching rate (1.5 nm min^{-1}) was achieved by depth profiling a Ta_2O_5 thin film of known thickness. Pressure in the sample chamber during this process was $\sim 10^{-7}$ Torr. Preferential sputtering effects may cause some variation in the quantitative profile results,[5] but no corrections were made. Depth–composition profiles were obtained using the Co 2p, Cr 2p, Fe 2p, Ni 2p, W 4f, O 1s and C 1s lines. On the samples tested at 250 h, Co 3p, Cr 3p, Fe 3p and Ni 3p peaks were also included, because these transitions are less affected than peaks at higher energies by surface contamination and preferential sputtering effects.[3,4] However, no significant differences were seen between either kind of analysis. Some sputter-induced effects, such as dehydration of metal hydroxides and the reduction of the higher oxides of iron to FeO, have been reported.[6,7] On the other hand, it is known[2,4,8] that CoO and Cr_2O_3 are predominantly stable under ion sputtering.

RESULTS AND DISCUSSION

Very small weight losses have been obtained in Stellite-6 in both of the environments tested, as was to be expected in this high-corrosion-resistant alloy. In spite of these small weight losses, slight differences between both solutions could be observed because the weight loss measured (in mg dm^{-2}) in specimens tested in solution B ($pH_{290\,°C}$ 5.05) are higher than in solution A ($pH_{290\,°C}$ 7.4) [Fig. 1(a)]. Furthermore, corrosion is best reported as the corrosion rate (mg dm^{-2} day^{-1}), calculated for each test as the ratio between the weight losses and the exposure time [Fig. 1(b)]. In this case, the corrosion rate obtained in solution B clearly decreased when the exposure time changes from 250 to 1000 h. These results indicate that specimens tested in solution B showed more material dissolution, especially at the shortest test.

The XPS analyses were firstly made at the outermost surface of the samples, revealing that the main elements on the unsputtered sample surface were oxygen, carbon, chromium, iron, cobalt and nickel. No tungsten was found on the outer surface of the samples, which is in good agreement with some previous studies.[3,4,9]

The chemical shifts on the 2p core-line spectra revealed that the most probable species at the outermost surface of all the samples tested were the hydroxides $Co(OH)_2$ (with CoO as a minor component), FeOOH and $Ni(OH)_2$, rather than the oxidized forms,[6,10,11] although the following considerations must be taken into account. The Fe $2p_{3/2}$ peak position coincides with a mixture of FeOOH as the predominant species and Fe_2O_3 or spinel-type oxides.[6,11–14] However, because the peak position for spinel-type oxides covers a range of energies from 710.6 to 711.4 eV,[6,13,14] we cannot discard the presence of some spinel-type oxides. In addition, the partial overlapping between the high Cr LMM Auger transition and the characteristic satellite (~8 eV above the Fe $2p_{3/2}$ peak) of

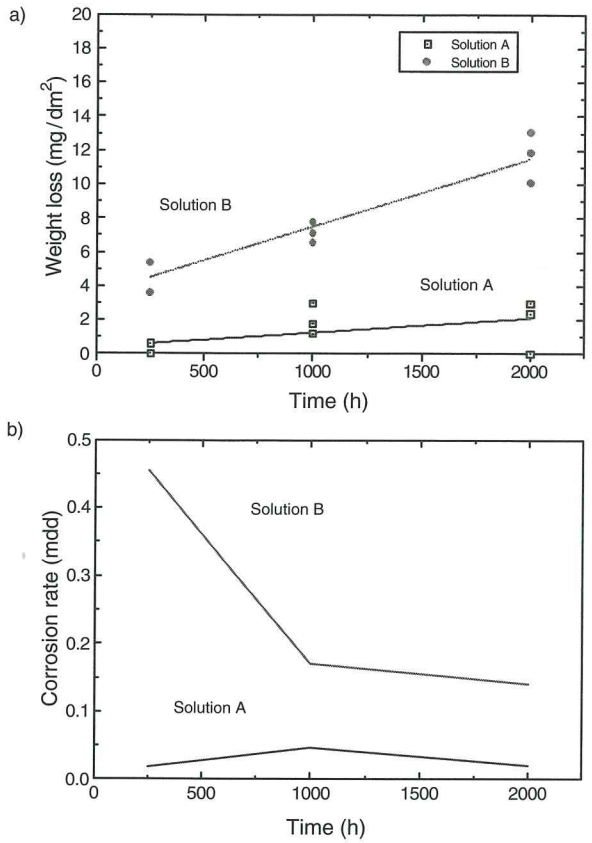

Figure 1. Results of corrosion tests of Stellite-6 tested in solution A (300 ppm H_3BO_3 + 2.65 ppm LiOH + 2 ppm H) and solution B (2000 ppm H_3BO_3 + 2 ppm H_2); (a) weight-loss measurements (mg dm^{-2}); (b) corrosion rates (mg dm^{-2} day^{-1}).

FeOOH and Fe_2O_3 does not permit us to discard the existence of any of these compounds. In spite of there being no clear distinction between chromium oxide and hydroxide, it seems that chromium appears as a mixture of CrOOH and Cr_2O_3,[7,15,16] which have been generally reported to form the passive layer of chromium alloys in accordance with thermodynamic predictions.[17] If considering the Cr $2p_{3/2}$ and O 1s peak positions, it seems that CrOOH is the most probable compound for samples exposed to solution A but Cr_2O_3 is the most probable species for samples exposed to solution B. However, a complete and unequivocal characterization was not possible.

The XPS depth profiles showed the development of a chromium-enriched cobalt-depleted oxide film, which was thicker in samples exposed to solution B ($pH_{290\,°C}$ 5.05) in comparison with those exposed to solution A ($pH_{290\,°C}$ 7.4). As an example of these profiles, Figs 2 and 3 show the depth profiles obtained for 2000 h tests in solutions A and B, respectively. The average thickness of the oxide layer was approximately constant (~75 nm) for samples A, but for samples B was smaller for the sample exposed to 250 h (~150 nm) than for the samples exposed to 1000 and 2000 h (~350 nm). The average thickness was estimated by taking into account the point at which the elemental concentration of the main alloy components was in good agreement with the nominal composition. The larger thickness of the oxide layers in samples B and the weight loss results would be consistent with the fact that solution B is slightly more corrosive than solution A. Moreover, the increase of the oxide layer thickness from 250 to 1000 h in the samples exposed to solution B

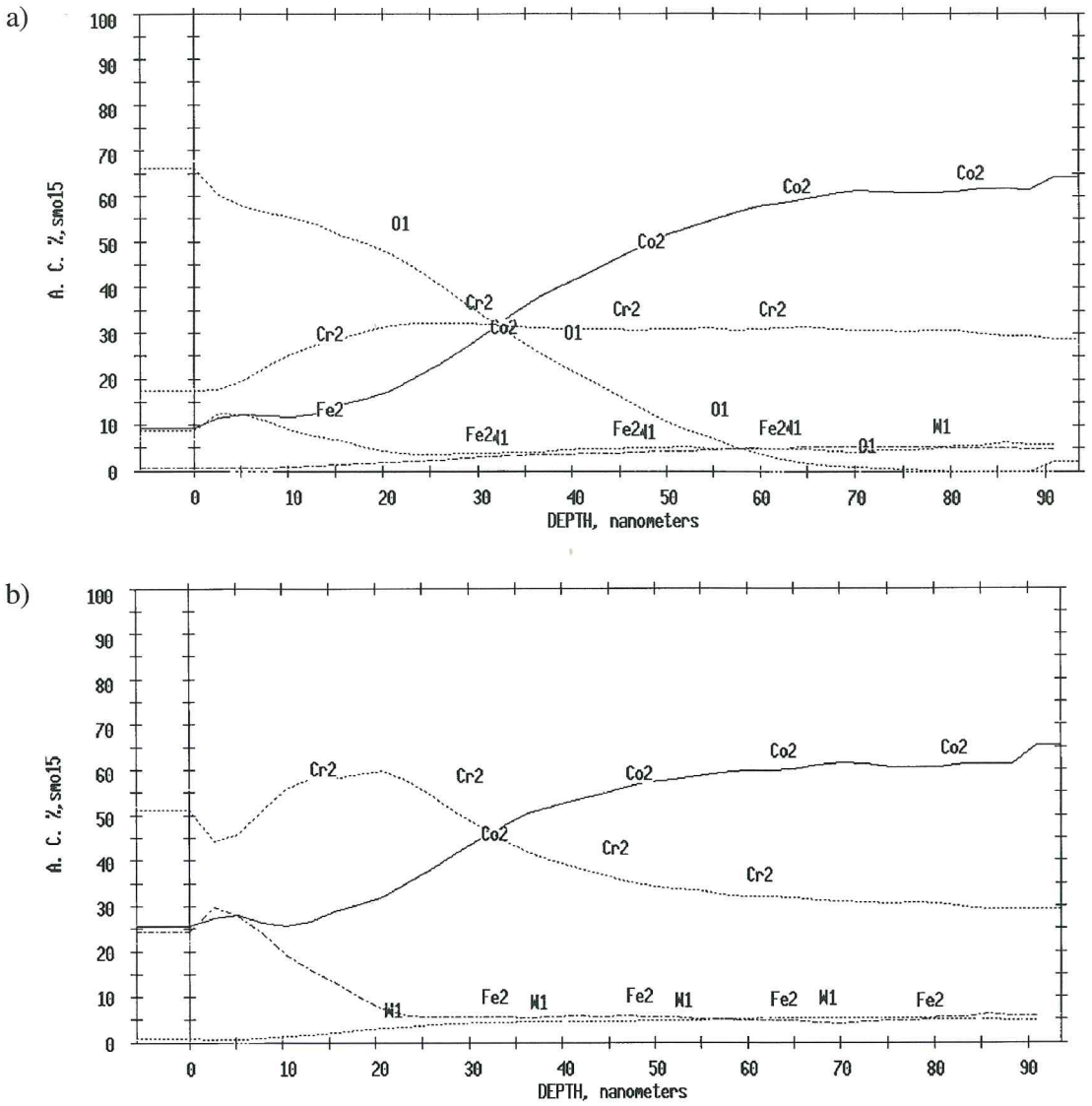

Figure 2. Depth profile of Stellite-6 tested in solution A (300 ppm H_3BO_3 + 2.65 ppm LiOH + 2 ppm H_2) for 2000 h: (a) Co, Cr, Fe, W and O normalized to 100%; (b) Co, Cr, Fe and W normalized to 100%.

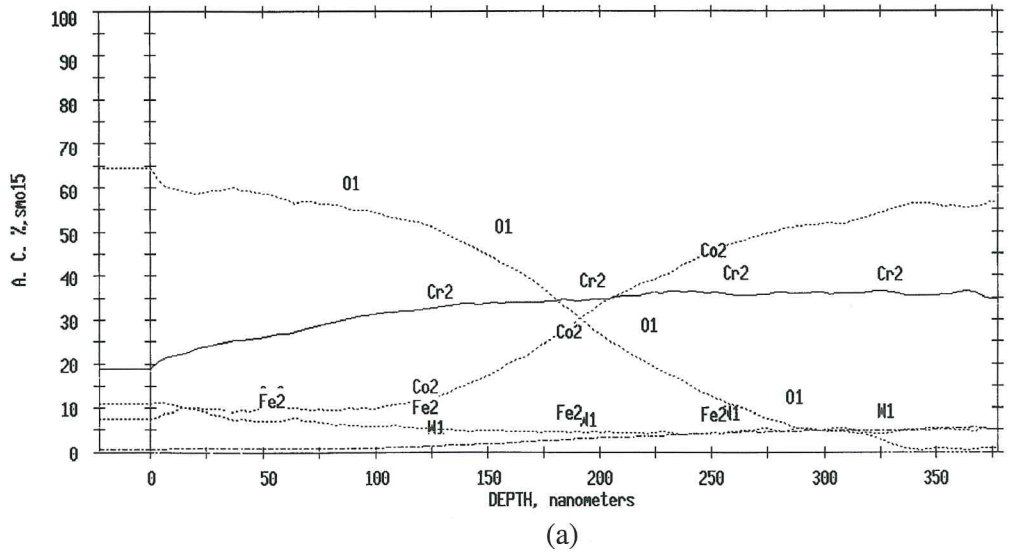

(a)

Figure 3. Depth profile of Stellite-6 tested in solution B (2000 ppm H_3BO_3 + 2 ppm H_2) for 2000 h: (a) Co, Cr, Fe, W and O normalized to 100%; (b) Co, Cr, Fe and W normalized to 100%.

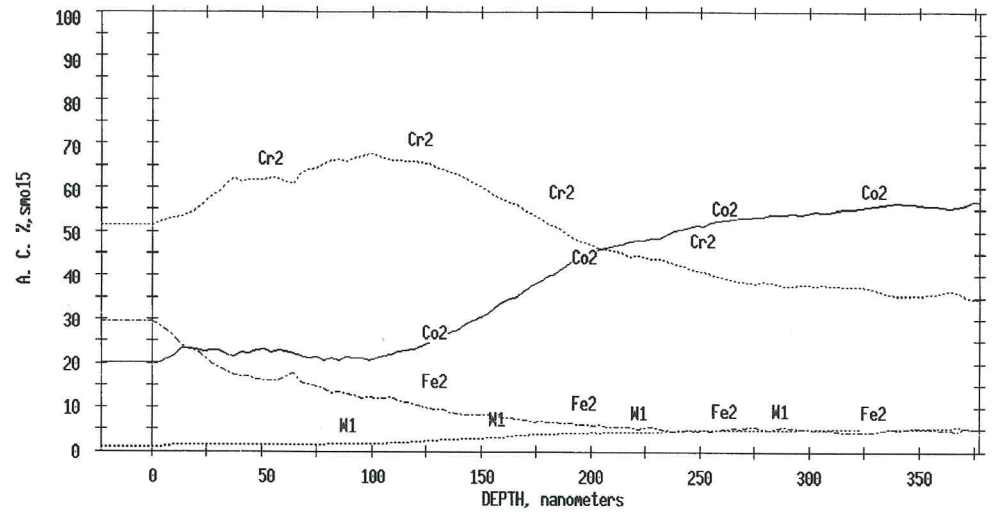

(b)

Figure 3. (*continued*).

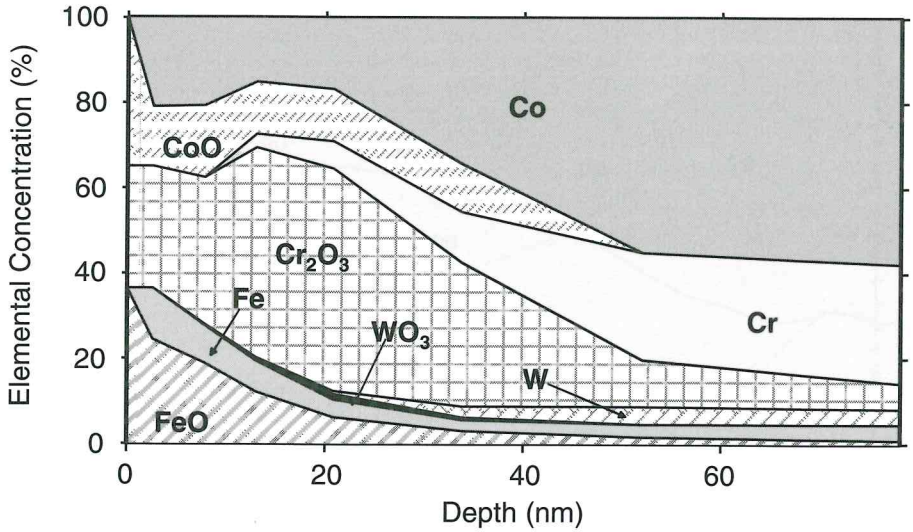

(a)

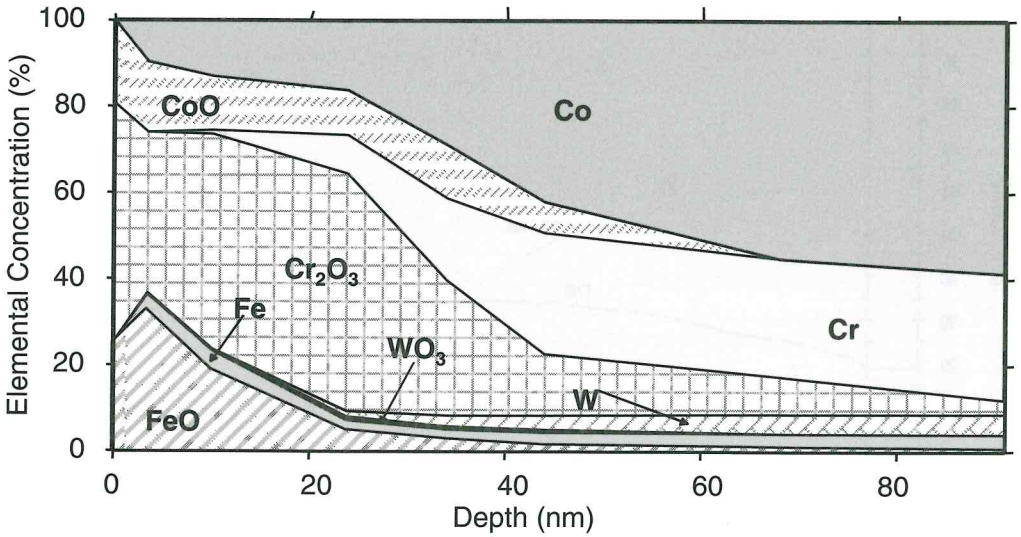

(b)

Figure 4. The XPS composition–depth profile of Stellite-6 tested in solution A (300 ppm H_3BO_3 + 2.65 ppm LiOH + 2 ppm H_2): (a) 250 h of testing; (b) 2000 h of testing.

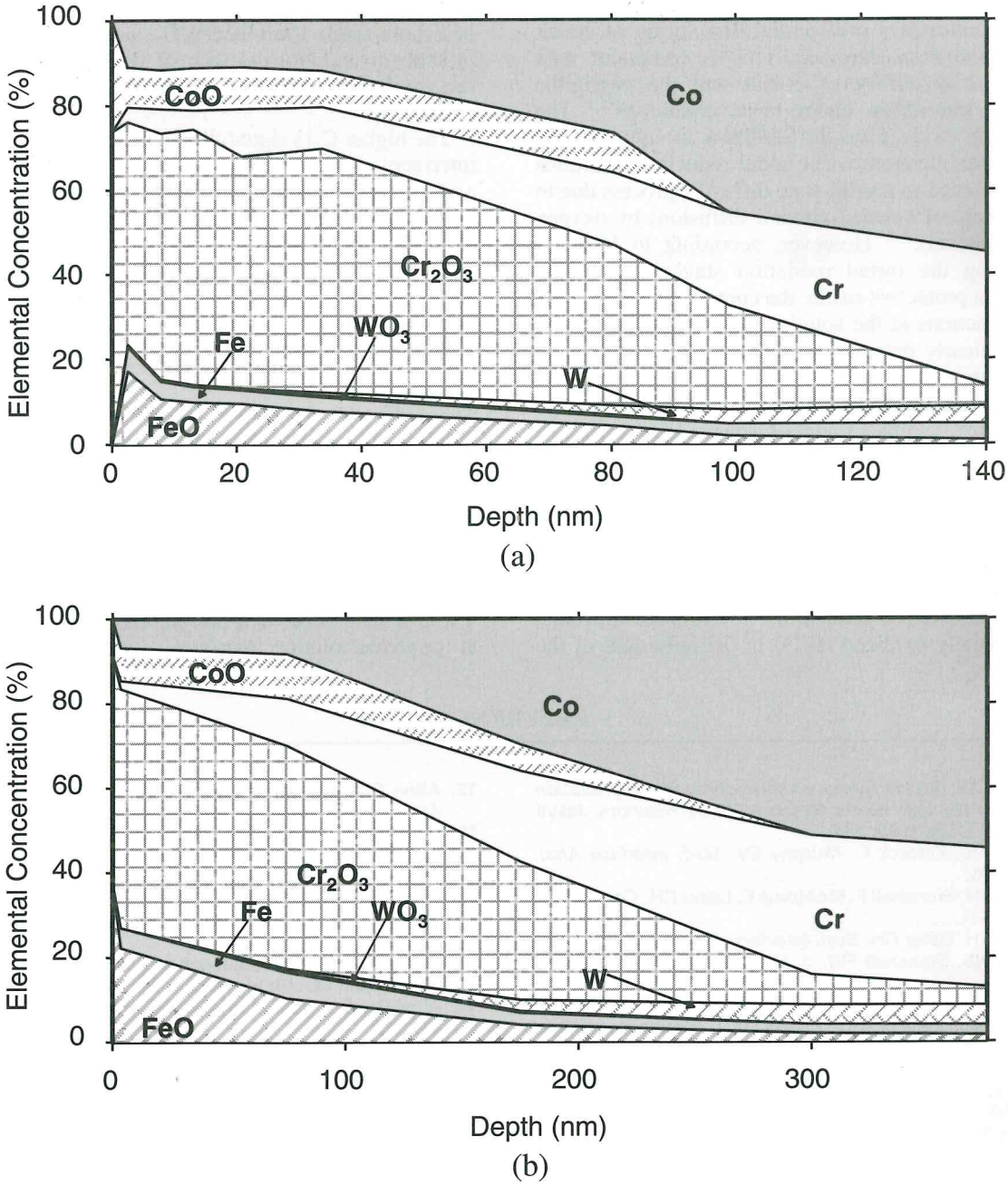

Figure 5. The XPS composition–depth profile of Stellite-6 tested in solution B (2000 ppm H_3BO_3 + 2 ppm H_2): (a) 250 h of testing; (b) 2000 h of testing.

and their corresponding weight loss values suggest that a protective film was not already formed at 250 h.

Figures 4 and 5 show the XPS composition–depth profiles, with separate oxidized and metallic forms, for samples tested at 250 and 2000 h in both environments. These profiles have been obtained by plotting cumulatively on the ordinate the relative metal concentrations. The accurate chemical form of the oxide cannot be determined because of ion-sputtering-induced effects, as mentioned above.[6,7] For this reason, we followed the procedure of McIntyre *et al.*,[2] Hocking *et al.*,[3,4] and Taylor and Annson,[9] i.e. to label the oxide phases according to the most stable species (CoO, Cr_2O_3, FeO) under ion etching.[2–8]

In spite of the mentioned thickness differences, there were no significant changes in the qualitative oxide composition. In both conditions, no cobalt oxide was detected close to the alloy surface. This seems to indicate, according to McIntyre *et al.*,[2] that cobalt ions are being dissolved preferentially in the solution as rapidly as they diffused to the interface. A subtle difference could be seen between both environments: metallic chromium was evident within a few monolayers of the outermost surface only for exposures to solution B, whereas for samples exposed to solution A it was detected some nanometres beneath the outermost surface, when the cobalt concentration began to increase at the expense of oxygen (see Figs 2 and 3). Another difference was that the cobalt content in the oxide layers was slightly higher for samples A. This fact seems to be in accordance with the higher thermodynamic stability of CoO in this environment.[18]

Thus, under both chemistry regimes, chromium-enrichment and cobalt depletion were evident within the oxide

film. The formation of this strongly chromium-enriched oxide layer indicates a preferential dissolution of cobalt at the oxide/solution interface. This is consistent with the significant solubility of cobalt and the negligible solubility of chromium under these conditions.[2,3] The growth of the oxide films in Stellite-6 in lithiated and borated high-temperature water under reducing conditions has been attributed to a solid-state diffusion process due to the replacement of cobalt (outward diffusion) by oxygen (inward migration).[2–4] However, according to Hocking *et al.*,[3] during the initial oxidation stages, before the formation of a protective oxide, the controlling factor must be kinetic reactions at the solution/surface interface.

Iron was clearly detected at the outermost surface and within the outer half of the oxide layer. In addition to the iron coming from the base material, by diffusion through the oxide lattice,[19] some amount of iron could be attributed also to the stainless-steel loop.[3,4] Notwithstanding that nickel was not included in the graphs, to make them clearer, this element was detected at very low concentrations throughout the oxide film in the whole set of samples tested. Only elemental nickel was detected in all cases, i.e. in accordance with the known fact of $NiO/Ni(OH)_2$ substantial sputter-induced reduction.[5,8,10,20] As for tungsten, it was completely oxidized (W^{6+}) in the outer half of the corrosion layer. McIntyre *et al.*[2] postulated the possibility of a more stable form than WO_3, such as cobalt tungstate, in order to explain the lack of reduction under sputtering conditions observed for the tungsten detected in his analyses.

The higher C 1s signal detected close to the oxide/metal interface at ~282.8 eV, the microstructure of the sample and the fact that metal and carbide are not distinguishable by XPS for W 4f and Cr 2p lines,[21,22] suggest that a mixed chromium–tungsten carbide was also possible near the oxide/metal interface and beyond.

CONCLUSIONS

The corrosion behaviour of Stellite-6 in lithiated and borated high-temperature water ($pH_{290\,°C}$ 7.4 and 5.05) under reducing conditions has been studied. Differences in the thickness of the oxide layers formed in the two solutions have been observed but no significant changes in the qualitative oxide composition have been detected. Under both chemistry regimes, chromium enrichment and cobalt depletion have been found between the oxide film. These results point to a preferential dissolution of cobalt at the oxide/solution interface.

REFERENCES

1. Comley GCW. *4th Int. Symp. on Environmental Degradation Material in Nuclear Power Systems-Water Reactors*, Jekyll Island, GA, USA, 1989; 3–1.
2. McIntyre NS, Zetaruk D, Murphy EV. *Surf. Interface Anal.* 1979; **1**: 105.
3. Hocking WH, Stanchell F, McAlpine E, Lister DH. *Corros. Sci.* 1985; **25**: 531.
4. Hocking WH, Lister DH. *Surf. Interface Anal.* 1988; **11**: 45.
5. McIntyre NS, Stanchell FW. *J. Vac. Sci. Technol.* 1979; **16**: 798.
6. McIntyre NS, Zetaruk DG. *Anal. Chem.* 1977; **49**: 1521.
7. McIntyre NS, Zetaruk DG, Owen D. *J. Electrochem. Soc.* 1979; **126**: 750.
8. Kim KS, Baitinger WE, Amy JW, Winograd N. *J. Electron Spectrosc. Rel. Phenom.* 1974; **5**: 351.
9. Taylor NK, Armson I. *Water Chemistry of Nuclear Reactor Systems 3*, vol. 1. BNES: London, 1983; 141–151.
10. McIntyre NS, Cook MG. *Anal. Chem.* 1975; **47**: 2208.
11. Allen GC, Curtis MT, Hooper AJ, Tucker PM. *J. Chem. Soc. Dalton* 1974; 1525.
12. Allen GC, Tucker PM, Wild RK. *Philos. Mag. B* 1982; **46**: 411.
13. Allen GC, Harris SJ, Jutson JA. *Appl. Surf. Sci.* 1989; **37**: 111.
14. Allen GC, Hallam KR. *Appl. Surf. Sci.* 1996; **93**: 25.
15. Allen GC, Curtis MT, Hooper AJ, Tucker PM. *J. Chem. Soc. Dalton*, 1973; 1675.
16. Halada GP, Clayton CR. *J. Electrochem. Soc.* 1991; **138**: 2921.
17. Beversdog B, Puigdomenech I. *Corros. Sci.* 1997; **39**: 43.
18. MacDonald DD, Shierman GR, Butler P. *AECL* 1972; 4138.
19. Allen GC, Dyke JM, Harris SJ, Morris A. *Appl. Surf. Sci.* 1988; **31**: 220.
20. González-Elipe AR, Holgado JP, Alvarez R, Munuera G. *J. Phys. Chem.* 1992; **96**: 3080.
21. Moulder JF, Stickle WF, Sobol PE, Bomben KD. In *Handbook of X-ray Photoelectron Spectroscopy*, (2nd edn). Chastain J (ed.). Perkin-Elmer Corp., Physical Electronic Division: Eden Prairie, MN, 1992.
22. Stern KH, Rolison DR. *J. Electrochem. Soc.* 1990; **137**: 178.